Assessing virgin and reclaimed carbon fibre electrodes in structural batteries

Chemical Engineering Journal 521 (2025) 166504

Contents lists available at ScienceDirect

Chemical Engineering Journal

journal homepage: www.elsevier.com/locate/cej

Assessing virgin and reclaimed carbon fibre electrodes in structural batteries

James D. Randall [a], Aqeel Muhammad [a], Emma G. Hogan [a], Timothy Harte [a], Žan Simon [a], Bhagya Dhamarsiri [a], Leif E. Asp [b], Luke C. Henderson [a,*]

[a] Institute for Frontier Materials, Deakin University, Waurn Ponds, Victoria 3216, Australia
[b] Department of Industrial and Materials Science, Chalmers University of Technology, 41258 Göteborg, Sweden

ARTICLE INFO

Keywords:
Structural energy
Carbon fibre
Recycling
Composite

ABSTRACT

The integration of structural components with energy storage functionality is a promising pathway to attaining weight reduction in aircraft and electric vehicles. In this work, we present a structural lithium-ion full cell that utilizes a discontinuous recycled carbon fibre textile as a cathode, paired with a virgin twill-weave carbon fibre anode and embedded within an epoxy-based solid battery electrolyte (SBE) containing an LiTFSI:TEGDME solvate ionic liquid (SIL). Two carbon fibre architectures were evaluated in half-cell conditions for both the cathode and anode - a 60 GSM recycled non-woven and a 325 GSM twill-weave carbon fibre. Despite the lower mass-loading, the reclaimed non-woven carbon fibre outperformed the woven counterpart due to possessing superior ion accessibility, resin infiltration and active mass distribution. The evaluation of a hybrid full cell using a reclaimed carbon fibre cathode and twill-weave anode demonstrated stable cycling at C/20 with a specific capacity of 25 mAh g^{-1}, fabricated entirely under ambient conditions without the need for a glovebox or dry room. This scalable prepreg-inspired approach demonstrates the feasibility of multifunctional composite design under real-world conditions, whilst also valorising reclaimed carbon fibres.

1. Introduction

The global transition toward a fossil fuel-free society has resulted in unprecedented advancements in lithium-ion battery (LIB) technologies. This shift is evident in the rise of global electric vehicle (EV) sales, increasing from 1 million units in 2014 to over 11 million in 2022, with projections exceeding 30 million by 2030 [1–4]. Despite state-of-the art LIB technologies achieving energy densities as high as 693 Wh L^{-1} [4–7], they remain inferior to its fossil-dependant gasoline counterparts in regard to volumetric energy density. One strategy to improve LIB performance is through lightweight structural materials using carbon fibre reinforced polymer (CFRP) composites, which have seen increased use in this regard to reducing weight and increasing driving range [8–10].

More recently, and given their ability to reversibly intercalate lithium ions, carbon fibres have attracted interest for their dual functionality as a structural battery composite material, combining load-bearing capabilities with energy storage [11–14]. When embedded in an ionically conductive polymer, the resulting architecture forms a structural battery, capable of supplying electrical energy while replacing non-functional vehicle components. Theoretical studies in replacing non-load bearing components, such as the roof of an EV have shown mass savings of up to 20 % when replaced with a structural battery [15].

Initial structural battery designed embedded traditional LIBs within composite structures [9,12,13], which failed to fully capitalize on the intrinsic mechano-electrochemical synergy of load-bearing electrodes. Later efforts demonstrated structural half-cells with carbon fibre-based anodes and cathodes [14,16–18], though many relied on lithium metal which limited safety and scalability. In 2020, Moyer et al. reported a lithium-metal free structural battery using LFP-coated carbon fibres and an ionic liqud (ALiTFSI/EMIMBF$_4$) in an epoxy matrix, achieving an energy density of 36 Wh/kg and a modulus of 1.8 GPa [9]. A more recent example, and the first reported fully integrated structural battery, utilized a bisphenol-A ethoxylate dimethacrylate (BPAMA) based solid battery electrolyte reaching 75 Wh/kg over 1000 cycles [19].

However, while interest in multifunctional composites grow, there remains a major gap in application pathways for reclaimed carbon fibres, which are increasingly generated as waste from decommissioned

* Corresponding author.
E-mail address: Luke.Henderson@deakin.edu.au (L.C. Henderson).

https://doi.org/10.1016/j.cej.2025.166504
Received 29 May 2025; Received in revised form 9 July 2025; Accepted 26 July 2025
Available online 28 July 2025

CFRPs [16,17]. Despite advances in fibre reclamation technologies, recycled carbon fibre textiles remain heavily underutilized in high-value applications [17]. One potential application for reclaimed carbon fibres could be as electrodes for LIBs, particularly due to the porosity of the reclaimed materials (Fig. 1a).

Unlocking the potential in energy storage could offer both technological and environmental benefits, aligning structural battery research with circular economy goals. To this end, we evaluate two distinct carbon fibre types – a discontinuous non-woven recycled carbon fibre mat (60 GSM) and a virgin twill-weave carbon fibre fabric (325 GSM) – to explore their suitability as electrode scaffolds for structural batteries. Both carbon fibres are PAN-derived, which are known to provide an excellent balance between mechanical strength (4–7 GPa tensile strength, and 230 GPa Young's modulus) and specific capacities of (250–350 mAh g^{-1} at C/10) [17]. As a comparison pitch-based fibres offer greater stiffness (up to 700 GPa) at the expense of electrochemical storage capacity (~150 mAh g^{-1}) [18–20].

Furthermore, the practical fabrication of a structural battery under standard composite manufacturing conditions remains a significant challenge. For example, batteries are typically assembled in a glove box, providing an oxygen and water free environment, while composites are typically manufactured open to the air using pre-impregnated materials. This mismatch in processing requires either a significant shift in the composite manufacturing process, or the development of new electrolytes that can tolerate moisture [21,22]. Therefore, this work seeks to determine if a working structural battery can be fabricated successfully in typical composite manufacturing conditions. Other challenges include active cathode material coating homogeneity, low mechanical strength of the solid battery electrolyte (SBE) matrix, and poor adhesion of carbon fibres to the SBE and active cathode particles [23–27].

As global LIB and CFRP composite demands continuous to rise, the integration of recycled carbon fibres in new applications are imperative to reduce global waste and ensure a sustainable global future. This work reports the first structural full-cell battery that utilizes discontinuous recycled carbon fibre textiles (6 mg cm^{-2}) in the cathode, in the form of a carded non-woven fabric.

Here a hybrid structural battery is fabricated that utilizes the high volumetric space of the recycled carbon fibre to allow more LFP integration than a standard twill-weaved carbon fibre fabric (32.5 mg cm^{-2} areal density). In parallel we introduce a solid battery electrolyte (SBE) based on equimolar LiTFSI and tetraethylene glycol dimethyl ether (TEGDME) solvate ionic liquid (SIL) embedded in epoxy. SILs are non-volatile, flame-resistant, and thermally stable – key attributes for structural composite integration [28,29]. Moreso, we have recently shown that the resulting SBE can be effectively recycled using environmentally friendly solvents (ethanol), and with high mass recovery (>90 %) [30].

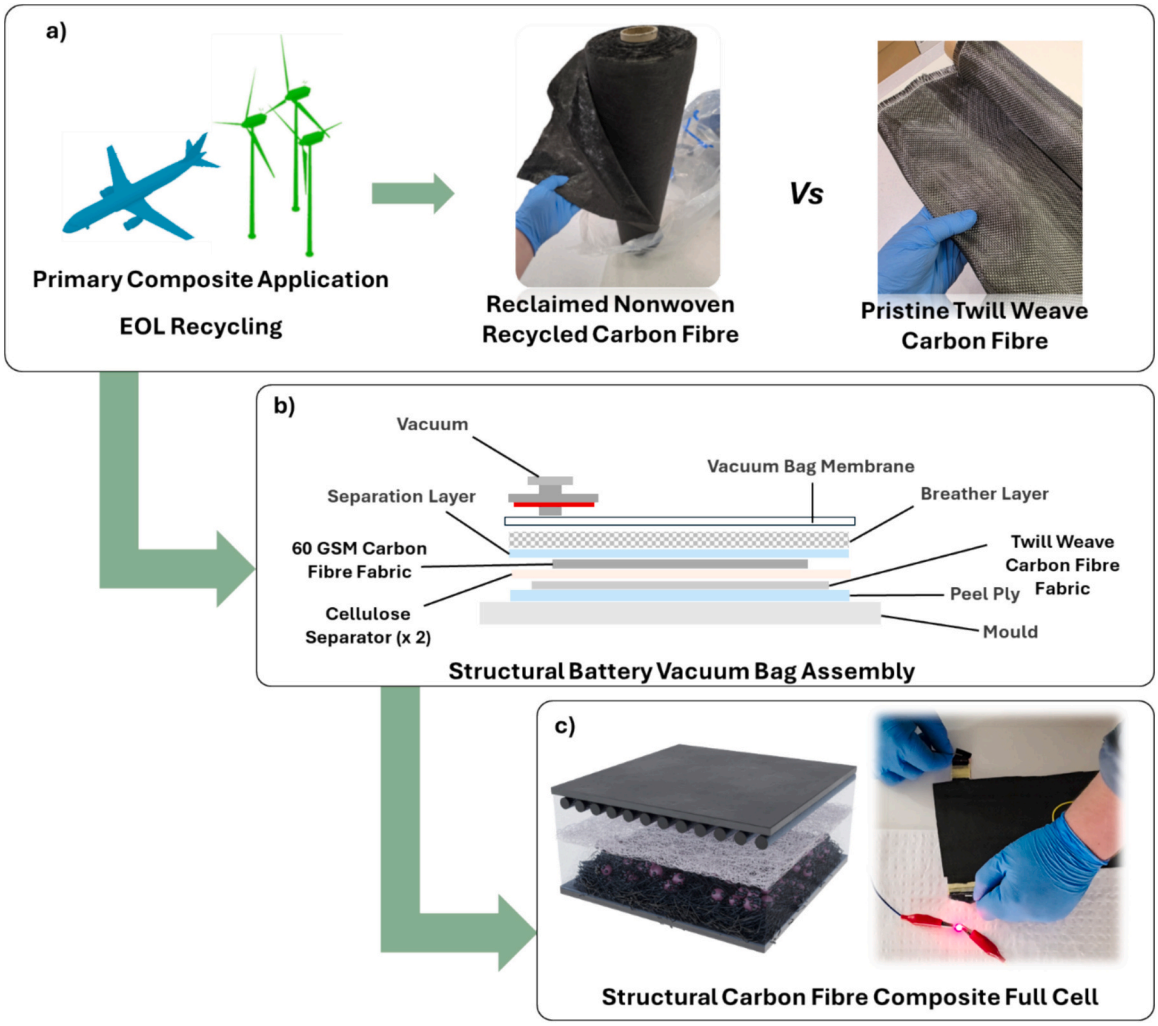

Fig. 1. Schematic of structural full cell assembly using reclaimed carbon and pristine twill weave carbon fibres with an G4:LiTFSI ionic liquid epoxy blended solid battery electrolyte (SBE). (a) raw materials and chemical structures, (b) vacuum bagging process to develop the structural battery and (c) demonstration of the structural battery holding charge and lighting an LED light.

2. Materials and methods

2.1. Materials

Carbon fibre PAN type was sourced from Toray (FT300B) and were desized by Soxhlet extraction in refluxing acetone for 48 h. The fabrics had an approximate density of 32.5 mg cm^{-2} and were used in the manufacture of the carbon fibre structural anode half-cell and composite full cells. Discontinuous recycled non-woven carbon fibre (60 GSM) was sourced from Gen 2 Carbon Ltd. and were used as received for the manufacture of structural cathodes and composite full cells. Conductive carbon adhesive (502) was purchased from Electron Microscopy Sciences (Hatfield, PA, United States). $LiFePO_4$ powder was supplied by mKube Enterprise Pty Ltd. and had a particle size of 5 μm. Copper foil (9 μm thickness), Aluminium foil (16 μm thickness), Aluminium laminated foil for pouches, nickel and aluminium tables (0.1 × 5 × 45 mm), Polypropylene PP separator (20 μm thickness) and cellulose separators (29 μm thickness, battery grade, 7 cm width), 2032 coin cell casings, spring and spacers were also purchased form mKube Enterprise Pty Ltd. Conductive Super P carbon black (CB, ≈40 nm), Lithium bis(trifluoromethanesulfonyl)imide (LiTFSI) and Tetraethylene glycol dimethyl ether (TEGDE) were sourced from Sigma-Aldrich and dried before use. All other chemicals and solvents were sourced from Sigma-Aldrich and used without further purification.

2.2. Solvate ionic liquid preparation

The solvate ionic liquid (SIL) [Li-G4]TFSI was synthesized according to previously published reports by combining equimolar quantities of tetraethylene glycol dimethyl ether [G4] and lithium bis-(trifluoromethanesulfonyl)imide (LiTFSI) [31,32]. In this case, the two reactants were stirred at room temperature for 24 h, followed by drying under high vacuum for 3 h at 120 °C to remove residual water and used without further purification.

2.3. Synthesis of structural anode

The anode slurry mixture was prepared by combining 10 g of an equimolar (1:1) mixture of G4:LiTFSI ionic liquid with 366.4 mg of CB and stirred in a sealed vial for 48 h at room temperature. Electrode assembly comprised of a composite vacuum bag setup starting with a release layer at the bottom, a 90 × 70 mm sheet of copper foil (9 μm thickness), a 90 × 70 mm CF fabric (60 GSM non-woven recycled or 320 GSM 'virgin' twill-weave), a release peel-ply and lastly a breather fabric. To form the SBE, RIM 935 (3.31 g) and RIM 936 crosslinker (0.97 g) were mixed thoroughly for 5 min and degassed under vacuum for 15 min. The anode slurry mixture was then mixed with the epoxy to give a final CB content of 2.5 wt%. The resulting mixture was then evenly brushed onto the carbon fibres and coated on both sides, before being centred on the copper foil current collector. The fibre and foil were then sandwiched between two release films (peel ply), followed by a breather layer and vacuum membrane on top. A notch for a vacuum valve was then placed and the whole system sealed using vacuum sealant tape. Finally, a strong vacuum was applied, facilitating the flow of resin through the composite and into the breather. The system was left under vacuum for 48 h to allow for a full resin cure. Afterwards, the composite anode was removed from the vacuum bag setup, and 10 mm diameter disks were punched and weighed, followed by transferal into a glovebox for half-cell assembly.

2.4. Synthesis of structural cathode

For the non-woven structural cathode, a slurry mixture was prepared by combining 10 g of equimolar (1:1) mixture of G4:LiTFSI ionic liquid with 1.63 g of $LiFePO_4$, 366.4 mg of CB in a sealed vial and stirred for 48 h at room temperature. Electrode assembly comprised of a composite vacuum bag setup starting with a release layer at the bottom, a 90 × 70 mm sheet of aluminium foil (16 μm thickness), a 90 × 70 mm CF fabric (60 GSM non-woven recycled fabric), a release peel-ply and breather fabric. RIM 935 (3.31 g) and RIM 936 crosslinker (0.97 g) were mixed thoroughly for 5 min and degassed under vacuum for 15 min. To form the SBE, the $LiFePO_4$ slurry was combined with the epoxy and stirred thoroughly for 5 min. The final $LiFePO_4$ content was 10 wt% with a carbon black content of 2.25 wt%. The SBE was evenly brushed onto the CF textile and coated on both sides, before being centred onto the aluminium foil current collector. The fibre and foil were then sandwiched between two release films (peel ply), and a breather layer added over the whole system. A notch for a vacuum valve was then placed and the whole system sealed using sealant tape and a vacuum bag membrane. Finally, vacuum was applied that facilitated the flow of resin through the composite into the breather layer. The system was left under vacuum for 48 h to allow for a full resin cure. Afterwards, the composite cathode was removed, and 10 mm diameter disks were punched out, weighed and transferred into a glovebox for half-cell assembly.

The twill-weave woven cathode followed a similar process, however a greater amount of LFP particles was needed to attain comparable LFP loadings. Consequently, 6.28 g of LFP particles was needed, resulting in 30 wt% LFP content and 1.75 % CB.

2.5. Glovebox assembly of composite half coin cells

Composite electrode disks were transferred into an argon filled glovebox with O_2 and H_2O levels <0.1 ppm. The electrolyte solution was either a solution of 1 M $LiPF_6$ in ethylene carbonate (EC) and diethylene carbonate (DEC) (1:1 v/v), or the equimolar (1:1) G4:LiTFSI electrolyte. Starting with the positive terminal case, the electrode disk was placed and electrolyte (700 μl) added dropwise onto the electrode surface. Following this, a polypropylene separator (mKube Enterprise Pty Ltd., 29 μm thickness) was placed gently on top, a 15.6 mm Li metal chip (mKube Enterprise Pty Ltd., 450 μm thickness), spacer and spring was then also placed in order. Lastly, the negative terminal case was placed and the cell subsequently crimped to ensure structural integrity. Following an overnight stabilization period, the assembled cell was then used for electrochemical testing.

2.6. Assembly of structural full cells

Anode and cathode electrodes were prepared similarly to Sections 2.3 and 2.4 with some alterations to cure-time and some initial sample preparatory steps. The cathode electrode slurry mixtures were prepared by mixing 10 g of equimolar (1:1) of G4:LiTFSI ionic liquid with 1.63 g of $LiFePO_4$ and 366.4 mg of carbon black in a sealed vial, likewise the anode slurry mixture comprised of 10 g equimolar (1:1) of G4:LiTFSI ionic liquid with 366.4 mg of carbon black, both were stirred for 48 h at room temperature. Meanwhile, 4 separate non-woven and twill-weaved CF fabrics were cut to 20 × 20 mm dimensions. The edges of the twill-weaved fabric were sealed with epoxy (Araldite, Selleys®) to prevent tow fraying and misalignment. Nickel and aluminium tabs (0.1 × 5 × 45 mm) were affixed at the corners of each electrode with approximately 20 mm protruding outwards and a small amount of conductive carbon adhesive was used to affix the tabs to the fibre. The electrodes were then dried in a vacuum oven at 120 °C for 12 h.

Afterwards, RIM 935 (3.31 g) and RIM 936 crosslinker (0.97 g) were mixed thoroughly for 5 min and degassed under vacuum for 15 min. The SPE mixture was formed by combining the ionic liquid electrode slurry with the epoxy resin, stirring thoroughly for 5 min. Electrode assembly comprised of a composite vacuum bag setup starting with a release layer at the bottom, the 20 × 20 mm carbon fibre electrode (with nickel or aluminium tab protruding), a release peel-ply, a breather fabric and lastly a vacuum bag membrane. Before sealing, the SPE mixture was evenly brushed onto the CF and coated on both sides, before a vacuum was applied for 4 h to allow for partial curing and to remove any excess

resin.

10 min before the end of partial cure, more SBE mixture was prepared by combining 5 g of equimolar (1:1) G4:LiTFSI with RIM 935 Epoxy resin (1.66 g) and RIM 936 crosslinker (0.48 g). Afterwards, the electrodes were carefully removed from the vacuum bagging setup, and a second vacuum bagging step was initiated to form the structural full cell. A release film comprised the first layer and the partially cured cathode affixed on top. Approximately 2 ml of the SBE mixture was spread onto the surface of the cathode and 2 cellulose separators (cut to 60 × 70 mm and dried at 100 °C for 12 h under vacuum prior) were gently placed on top. Another 2 ml of SBE mixture was added dropwise onto the surface and the structural anode placed (fibre side facing the separator) centred with the cathode. A second release ply was layered, followed by a breather layer and vacuum membrane. Vacuum was pulled and the system left to cure for 48 h at room temperature. Finally, the structural full cells were obtained and sealed in vacuum sealer using a laminated aluminium pouch and subsequently used for battery testing.

Please refer to the ESI for fabrication of the encased structural full cell.

2.7. Electrochemical testing of carbon fibre structural batteries

Battery tester (Neware A211) and potentiostat (Biologic VMP-300) were used to examine the specific capacity at various C-rates, long term cycling, voltage vs specific capacity, CV curves and electrochemical impedance spectroscopy (EIS) data.

Galvanostatic charge/discharge (GCD) was conducted using a Neware battery tester (BTS8000), with cycling stability monitored up to 1000 cycles at C/20. The voltage range was between 0.01 and 1.5 V for the anode, 2.5–4.0 V for the $LiFePO_4$ cathode, and 2.0–3.65 V for the hybrid full cell. The selected current for GCD was based on the theoretical capacity of graphite (372 mAh g^{-1}) and the mass of the carbon fibre for the anode, whilst based on the theoretical capacity of $LiFePO_4$ (170 mAh g^{-1}) for the cathode and full cell. Specific capacity of the samples was calculated from the discharge curves as per the formula $\boldsymbol{Q = \int Idt/m}$, where Q is the specific capacity (in mAh g-1), I is the current applied and m is the mass of the CF active material [33]. Moreover, the coulombic efficiency (CE) is known as ratio between prepared cell discharge and charge capacity during the same cycle. Hence, CE provides the ratio between total Li-ions insertion into anode material and total Li-ions back to cathode material [34]. Cyclic voltammetry (CV) and electrochemical impedance spectroscopy (EIS) were conducted on a Bio-Logic SP-300 station. CV of half cells were performed at various scan rates (0.2 to 409.6 mV s^{-1}) with a voltage range of 0–3.0 V for 3 cycles each for the anode, whilst 2.3–4.0 V for the cathode and full cell. EIS measurements were performed over a frequency region of 100 kHz to 100 mHz using a single sine alternative current (AC).

2.8. Cross-sectional scanning electron microscopy (SEM)

Cross-sectional morphology of the structural battery electrodes was examined using scanning electron microscopy (SEM). Surface characterization was conducted using a field emission scanning electron microscope (JEOL JSM-7800F) operated at an accelerating voltage of 15 kV. Energy-dispersive X-ray spectroscopy (EDX) was performed at the same voltage using an Oxford Instruments EDX detector to confirm the distribution of LFP particles within the electrode matrices.

2.9. Mechanical testing of carbon fibre full cells

For calculating the tensile strength and Young's Modulus, SBE-infused carbon fibre structural full cells were waterjet cut into dog-bone samples using dimensions outlined in ASTM D638 for Type V specimens, followed by drying in a vacuum oven at 80 °C for 12 h. Accordingly, the overall length of the specimen was 63.5 mm and the sample gage length 7.62 mm. The thickness of the full cells was on average 0.93 ± 0.19 mm, while the encased full cell was 2.09 ± 0.15 mm. Testing was carried out on a universal testing system (Instron 2 kN 5900 series, Illinois Tool Works Inc), at a testing speed of 0.1 mm/min. 5 samples of each was tested, and the modulus, a strain was calculated by cross-head displacement. Modulus E was calculated using E = L/CA, where L was the specimen gauge length, A was the cross-sectional area, and C was the true compliance. The true compliance, C was determined from $C = C_a - C_s$, where C_a is the apparent compliance from the initial linear segment of the load-displacement curve, and C_s was the system compliance, measured experimentally.

Flexural properties were obtained using a 3-point bending setup following ASTM D790 procedure B type I. Sample dimensions were rectangular with a length of 50.8 mm, 12.7 mm width and thicknesses ranging from 0.85 ± 0.03 mm for the full cell and 2.13 ± 0.11 mm for the encased cell. The support span was 25.4 mm. Testing was carried out on a universal testing system (Instron 30 kN 5900 series, Illinois Tool Works Inc), at a testing speed of 0.1 mm/mm/min. 5 samples of each was tested, and the modulus, a strain was calculated by cross-head displacement. Flexural modulus E was calculated using the following equation:

$$E = \frac{L^3 m}{4bd^3}$$

where E = modulus of elasticity, MPa. L is the support span (mm), b is the width of the sample (mm), d is the sample thickness (mm) and m is the slope of the initial straight line portion of the load-deflection curve.

3. Results and discussion

To systematically evaluate the electrochemical viability of carbon fibre fabrics as multifunctional electrodes, we began by benchmarking the performance of free-standing non-woven carbon fibres in conventional half-cell configurations. This allowed us to isolate and assess the compatibility of the solvate ionic liquid (SIL) electrolyte with the reclaimed fibre. Following this, we progressed toward composite integration by embedding the fibres in an epoxy-based solid battery electrolyte (SBE), enabling direct comparison of woven and non-woven architectures in structural half-cell formats. The distinct textile morphologies provided an opportunity to explore the influence of fibre alignment, resin infiltration, and active material distribution on electrochemical behaviour.

3.1. SIL performance on free-standing carbon fibres: G4:LiTFSI vs $LiPF_6$

In our previous work G4:LiTFSI has been employed as a structural polymer electrolyte in supercapacitors, an evaluation of the influence of SIL content in epoxy resulted in a blend ratio of 70 wt% SIL in 30 wt% epoxy (including crosslinker) attaining the highest ionic conductivity and Young's Modulus (0.074 ± 0.007 mS cm^{-1} and 0.739 ± 0.07 GPa, respectively) [30,31]. Furthermore, TGA analysis showed no significant mass loss up to around 210 °C. Given the high ionic conductivity, mechanical strength and thermal stability of this system we were prompted to benchmark this SBE in terms of electrochemical performance in anode half cells. As such, the selected SBE (G4:LiTFSI in epoxy 70:30 wt%) was compared against commercially available $LiPF_6$-based electrolyte with free-standing carbon fibre anodes. Emphasis was placed on assessing the stability, electrode compatibility, and capacity retention when interfaced with carbon fibre electrodes. Recycled non-woven carbon fibres (60 GSM) were selected as the primary anode substrate, as they are self-supporting and can be readily evaluated within coin cells. In contrast, the virgin twill-weave carbon fibres exhibited poor fibre cohesion, making them difficult to handle without a supporting polymer electrolyte resulting in low data reproducibility, thus were omitted from this part of the study.

Evaluation of the electrolytes at various charge rates highlight the electrochemical performance advantages of the $LiPF_6$ electrolyte in comparison to the G4:LiTFSI (Fig. 2b). Commercial $LiPF_6$ electrolyte (in EC:DEC) exhibited a specific discharge capacity of 149.6 ± 3.0 mAh g^{-1} at C/10, with an initial irreversible capacity of 104.2 mAh g^{-1}, attributed to electrolyte decomposition during the formation of the solid electrolyte interphase (SEI). Subsequent cycles displayed no further capacity loss, indicating a stable SEI. In comparison, the G4:LiTFSI electrolyte delivered a specific discharge capacity of 67.6 ± 3.2 mAh g^{-1} at C/10, with an irreversible capacity of 53.9 mAh g^{-1} after the first charge. Although this represents a ~58 % reduction in capacity relative to $LiPF_6$, the high coulombic efficiency observed in later cycles suggests the formation of a similarly stable SEI.

Therefore, at a cost of approximately half cell capacity, the G4:LiTFSI electrolyte offers significant advantages including non-volatility and enhanced safety, which motivated further investigation into its performance in structural half-cells incorporating an epoxy-based solid electrolyte. Notably, cycling at higher charge rates revealed similar trends in capacity retention, with the $LiPF_6$ electrolyte achieving specific discharge capacities of 129.9 ± 0.9 mAh g^{-1}, 91.6 ± 2.2 mAh g^{-1}, 57.4 ± 0.8 mAh g^{-1}, and 21.9 ± 0.6 mAh g^{-1} at C-rates of C/5, C/2, 1.0C, and 2.0C, respectively. In comparison, the G4:LiTFSI electrolyte exhibited specific discharge capacities of 24.2 ± 0.5 mAh g^{-1}, 5.7 ± 1.1 mAh g^{-1}, 1.1 ± 0.8 mAh g^{-1}, and 0 mAh g^{-1} at the same rates.

3.2. Structural half-cell anode performance: woven vs non-woven

Following the successful demonstration of G4:LiTFSI solvate ionic liquid (SIL) electrolyte performance with free-standing non-woven carbon fibre anodes, efforts shifted toward developing a composite anode structure. This was achieved by blending the LiTFSI SIL with epoxy resin at a 7:3 weight ratio, with 2.5 wt% carbon black added to promote electronic conductivity across the structural battery electrolyte (SBE) matrix.

Two types of carbon fibre fabrics were investigated — first as half-cells, and later within full cell assemblies. The first was a reclaimed non-woven fabric with an areal density of 6 mg cm^{-2}, while the second was a virgin twill-weave fabric with a significantly higher areal density of 32.5 mg cm^{-2}. These are referred to hereafter as non-woven and woven fibres, respectively.

Although the woven fabric contained substantially more active material (i.e. density of carbon fibres), initial expectations of higher performance were not realised by electrochemical rate performance measurements. Charge–discharge profiles at various rates (Fig. 3a) revealed that the non-woven composite anode exhibited markedly better rate performance, delivering a specific discharge capacity of 116.8 ± 4.3 mAh g^{-1} at C/100—nearly four times that of the woven electrode, which gave only 30.5 ± 1.1 mAh g^{-1} under the same conditions. This difference is not solely a function of active mass; while the twill electrode contained approximately 5.6 times more fibre (25.5 mg vs. 4.5 mg), the more accessible architecture of the non-woven appears to facilitate faster and more efficient lithiation.

At low rates (C/100), the woven electrode achieved a higher areal capacity due to its greater mass loading (0.61 ± 0.02 mAh cm^{-2} vs. 0.44 ± 0.04 mAh cm^{-2}, Fig. 3b). However, at higher rates (C/10), the performance of the woven structure dropped sharply, delivering just 0.05 mAh cm^{-2}, while the non-woven maintained a higher value of 0.10 mAh cm^{-2}. This highlights the improved rate capability of the non-woven composite, where its more distributed fibre network provided better ionic accessibility and reduced transport limitations.

Further analysis of the state of charge (SOC) revealed that the woven electrode reached only ~20 % SOC at C/100, while the non-woven approached ~80 % under the same conditions. The woven anode can eventually reach a comparable SOC if cycled at C/500 (See Supplementary Information, Fig. S1); however, a single full cycle under these conditions requires approximately 275 h, underscoring the significant kinetic limitations associated with its dense fibre weave architecture. Analysis of the nonwoven long-term cycling data (Fig. 3c) shows no significant capacity fade over 1000 cycles, meaning that little significant degradation to the nonwoven carbon fibre structure or collapse of the composite material occurred during testing.

Electrochemical impedance spectroscopy (EIS) measurements (Fig. 4) further supported charge-transfer limitations and were conducted before and after formation cycling. The fitted two-time constant equivalent circuit model included the bulk resistance ($\mathbf{R_s}$), the resistance to lithium-ion transport through the SEI layer ($\mathbf{R_{sei}}$), the charge transfer resistance ($\mathbf{R_{ct}}$), and a Warburg element ($\mathbf{R_w}$) to account for ion diffusion. $\mathbf{R_s}$ represents the cumulative ohmic resistance of passive components within the cell, including the electrolyte, separator, and hardware (e.g., casing, springs, spacers).

Before cycling, both the twill and reclaimed non-woven anodes exhibited $\mathbf{R_s}$ values of approximately 12–15 Ω, indicating good overall conductivity and low bulk resistance. However, a large semi-arc was also observed, which extended to ~4000 Ω, reflecting substantial interfacial resistance. This feature is characteristic of graphite-based anodes and is attributed to the onset of SEI formation from electrolyte

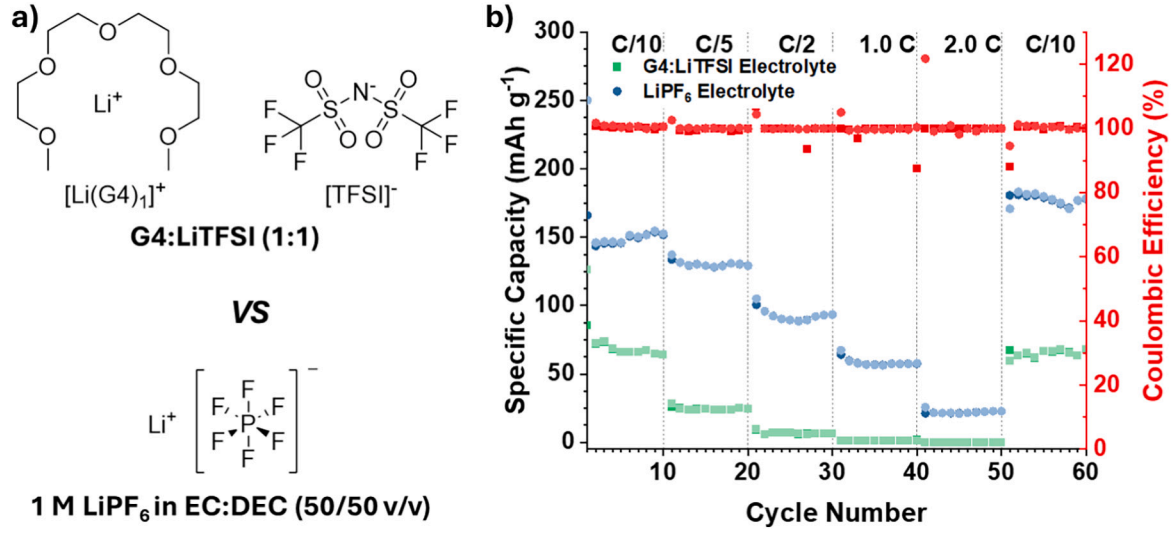

Fig. 2. (a) Chemical structures of the G4:LiTFSI liquid electrolyte (top) and $LiPF_6$ salt (bottom). (b) Comparative rate performance of the two electrolytes using non-woven carbon fibre as the anode.

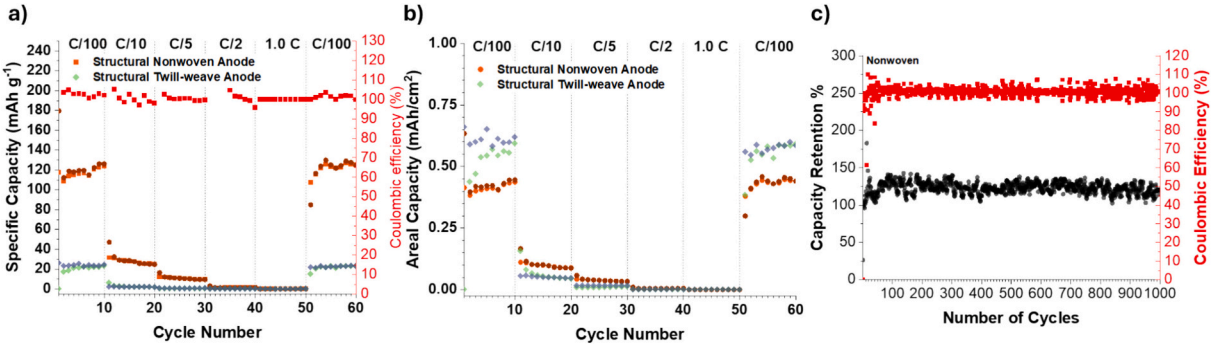

Fig. 3. (a) Electrochemical rate capability measurements of the non-woven and woven anode half-cells at C/100, C/10, C/5, C/2 and 1C respectively. (b) Areal capacity comparison of the woven (green) and non-woven (orange) electrodes across rates at C/100, C/10, C/5, C/2 and 1C. (c) Coulombic efficiency and capacity retention of nonwoven structural anode at C/10 over 1000 cycles.

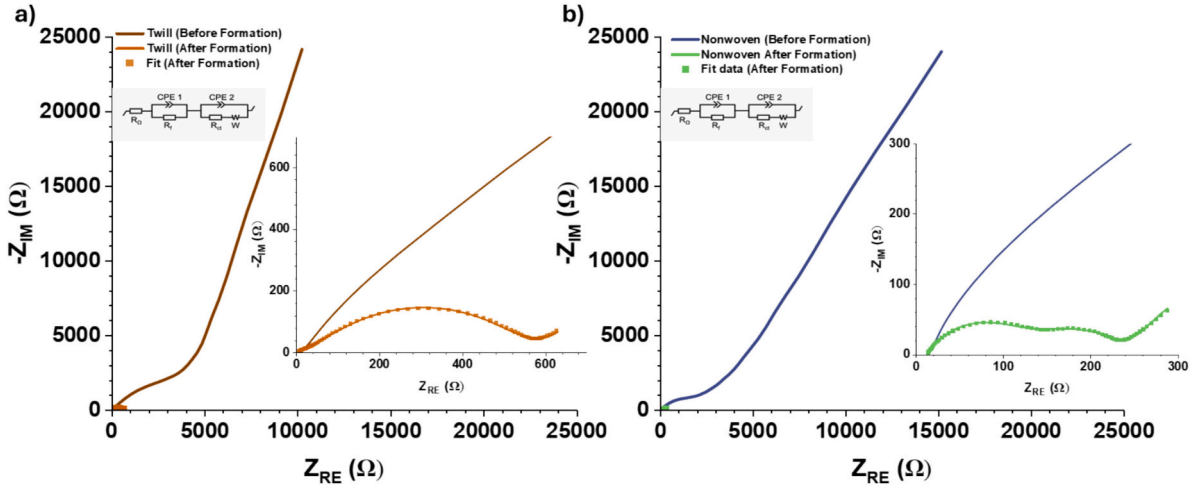

Fig. 4. Electrochemical Impedance Spectroscopy (EIS) measurements of the woven twill-weave composite anode (a) and the reclaimed non-woven anodes (b) before and after formation. EIS measurements were acquired between 100 kHz to 10 mHz.

decomposition [35–37]. At this stage, the SEI is not fully developed, resulting in capacitive blocking behaviour due to ion accumulation at the interface.

After formation cycling, the EIS response changed significantly. For the twill-weave carbon fibre anode, fitting revealed an SEI resistance ($\mathbf{R_{sei}}$) of 41.9 Ω and a charge transfer resistance ($\mathbf{R_{ct}}$) of 522.3 Ω. The higher $\mathbf{R_{ct}}$ suggests limited electrochemically active surface area, poor electrical contact within the electrode and weak infiltration and wetting of the SBE throughout the composite, likely contributing to its inferior rate performance observed above (Fig. 3). This was also observed by Siraj and coworkers, who noted considerable improvements in charge transfer by improving resin distribution and fibre alignment (Reducing $\mathbf{R_{ct}}$, from ~500 Ω to 75–150 Ω) [38,39]. In contrast, the reclaimed non-woven anode exhibited a higher SEI resistance of 126.1 Ω but much lower $\mathbf{R_{ct}}$ of 89.3 Ω, indicating more efficient charge transfer and better interfacial contact, this is consistent with more efficient lithiation of carbon fibres, observed at higher rates (up to C/5).

While the non-woven anode demonstrated superior rate performance, attributed to its more uniform fibre distribution and improved resin wettability, the twill-weave counterpart offers enhanced mechanical strength due to its aligned and densely packed fibre architecture [16,40]. This contrast prompted an investigation into the electrochemical behaviour of these same fibre types when employed as structural cathodes, with the goal of optimising both mechanical integrity and electrochemical performance in the resulting structural battery composite.

3.3. Structural half-cell cathodes: woven vs non-woven textiles

As with the structural anodes previously examined, both non-woven and twill-weave carbon fibre fabrics were explored as structural cathodes. Each was combined with a lithium iron phosphate (LFP)-embedded matrix to evaluate the impact on electrochemical performance within the composite architecture. Previous reports have utilized electrodeposition approaches to incorporate $LiFePO_4$ onto the surface of carbon fibres, the resulting coatings show relatively low polarization (39 mV overpotential at C/10) and high redox reversibility [41–43]. Whilst these methods have gained traction in recent years, high mass loadings (> 5 mg cm^{-2}) typically result in a reduction to cycle stability and energy density due to reduced particle adhesion at greater distances from the fibre, and variations in coating thickness (from 0 to 4 μm) relative to counter electrode distance [42]. Therefore, our search for higher and more well-distributed $LiFePO_4$ mass loadings prompted us to investigate dispersing $LiFePO_4$ particles directly into the solid battery electrolyte within a percolated conductive carbon black matrix (Fig. 1c). Impregnation of the carbon fibre fabrics with the mixture of epoxy/SIL/LFP/carbon black mixture provides a means of directly translating this to existing thermoset laminate prepreg manufacturing processes, whilst also allowing for rapid and scalable composite production (Fig. 5) [41].

We hypothesized that, in comparison to the conventional woven fibre that the random fibre arrangement of the recycled non-woven fibres allowed for greater resin and active material penetration during vacuum infusion process. In this way we had hoped to see improvements in the volumetric distribution and accessibility of LFP within the final

cathode product and thereby enhance charge storage capacity and rate performance. Before the full CF battery could be assembled each of the chosen fabrics, non-woven and woven, were both evaluated in a half-cell configuration to ensure that each of these materials worked in isolation, and to provide a preliminary reference point on the possible energy density.

Half-cell electrode fabrication (Fig. 5a) gave the non-woven composite cathode with an LFP areal density of 4.5 mg cm^{-2}, whereas the woven cathode attained approximately 3.5 mg cm^{-2}. Because the ionic liquid is also blended with an epoxy resin in the form of a solid polymer electrolyte (SPE), ionic mobility is constrained due to a tortuous path for ion migration, thus some degree of charge-transfer limitations was expected. Despite this, the 0.25 V peak-to-peak separation (Fig. 5b) of the non-woven cathode is approaching that of a conventional lithium-ion LFP cathode (~0.2 V), correlating to low kinetic limitations (resistances) within the cell and good ionic transport [44,45]. This contrasts with the woven composite cathode that exhibited a significant redox peak separation of 0.75 V (Fig. 5d), suggesting LFP particle distribution within the woven cathode experienced greatly reduced ion transport. Galvanostatic cycling (Fig. 5c, e) at 0.1C show marked differences in voltage profile behaviour between the woven and non-woven samples, reinforcing the observed contrasting electrochemical activity. A charge-discharge voltage difference of >0.5 V and a specific capacity of only 8 mAh g^{-1} was obtained for the woven cathode, whereas the non-woven showed much greater electrochemical activity - with a charge-discharge difference of only 0.1 V and a specific capacity of 54 mAh g^{-1} after the first cycle. Extended cycling over 350 cycles for both the non-woven and woven cathodes (Fig. 6) showcase reasonable stability of the SBE system - the nonwoven cathode exhibited a capacity loss of 25.5 %, whilst the woven 40.8 %. Much of this capacity loss occurred within the first 200 cycles and irrespective of fibre architecture, suggesting that potential LFP cracking or loss of conductivity through the conductive carbon network occurred.

Cross-sectional SEM images (Fig. 7a) reveal that the highly ordered and compact architecture of the twill-weave fibres limited the infiltration and uniform distribution of the solid battery electrolyte (SBE) within the composite. This resulted in the accumulation of LFP particles above and below the woven layers, impeding ion transport and leading to an overall increase in cell resistance. In contrast, the non-woven fabric facilitated a more homogeneous distribution of LFP particles throughout the composite (Fig. 7b), enabling improved ionic accessibility and more efficient electrochemical performance.

Galvanostatic charge-discharge cycling of the woven vs non-woven were measured at varying C-rates (Fig. 8b and c). The non-woven gave specific discharge capacities of 61.99 $mAhg^{-1}$ (C/100), 45.17 $mAhg^{-1}$ (C/10), 38.31 $mAhg^{-1}$ (C/5), 19.94 $mAhg^{-1}$ (C/2) and 9.66 $mAhg^{-1}$ (1C). This was significantly higher than the woven fabric which possessed discharge capacities of the woven at different rates are 10.26 $mAhg^{-1}$ (C/20), 4.04 $mAhg^{-1}$ (C/10), 1.01 $mAhg^{-1}$ (C/5), 0 $mAhg^{-1}$ (C/2, 1C and 2C). Again, this is consistent with the observations above suggesting that the non-woven fibres provide a superior material for electrochemical performance.

The rate capacity measurements show good columbic efficiency for both electrodes, yet the non-woven consistently outperforms the woven, achieving approximately 10 times higher capacity at C/10. Even at 1C, the non-woven fabric cathode maintains a specific capacity almost twice that of the woven composite cathode at C/20. These findings clearly demonstrate the superior rate capability of the non-woven electrode compared to its woven counterpart, particularly at higher C-rates where the woven fabric fails to deliver any measurable capacity. This can further be seen in the Randles–Ševčík plots (Fig. 8a), as both samples show linear slopes, indicating good reversibility. However, the non-woven fabric exhibits an oxidation slope (K_a = 0.117) nearly 5 times greater than the woven electrode (K_a = 0.0207), thus the non-woven cathode has significantly better ionic and electronic accessibility and less kinetic hindrance than its woven counterpart. It is important to note that while the Ka slopes can be used as a qualitative comparison on accessible charge pathways and reversibility, we opted against directly calculating diffusion rates due to several uncertainties (varied ion-path tortuosity, solid electrolyte interactions and heterogenous surface area).

Electrochemical impedance spectroscopy (EIS) of the LFP cathodes after several cycles further supported these findings (Fig. 9a and c). The

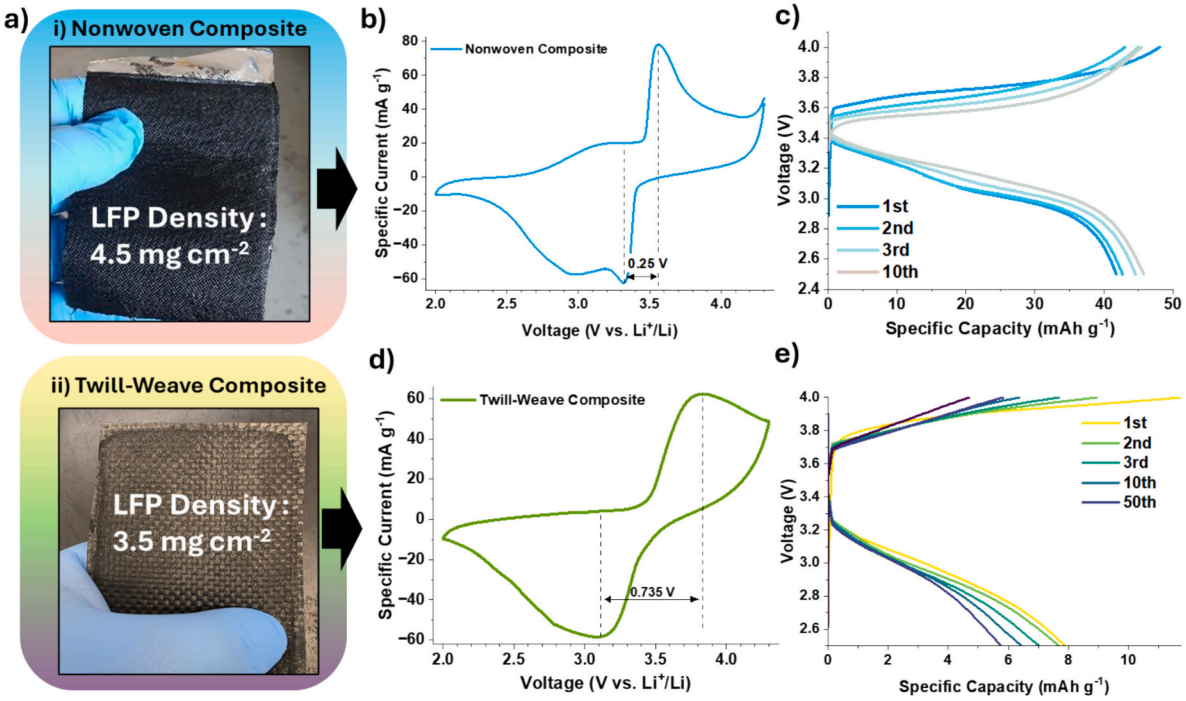

Fig. 5. (a) Photographs of the composite electrodes: (i) non-woven and (ii) twill-weave. (b) Cyclic voltammetry (CV) of the assembled non-woven half-cell at 0.1 mV s^{-1}. Voltage profile (c) versus specific capacity of the non-woven electrode at C/10. (d) CV of the twill-weave half-cell at 0.1 mV s^{-1}, and (e) corresponding voltage profile of the twill-weave composite cathode.

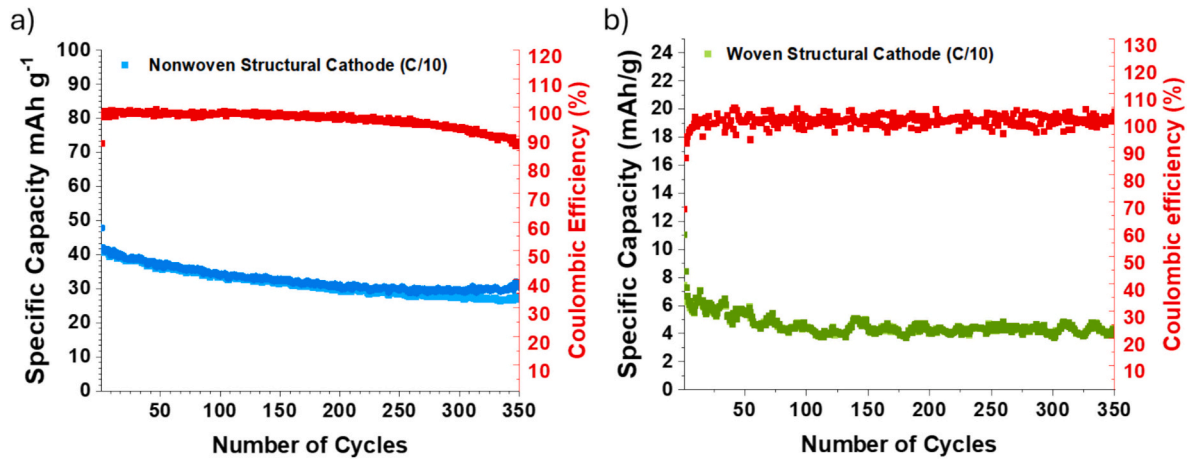

Fig. 6. Extended cycling of (a) nonwoven structural half-cell and (b) woven structural half-cell.

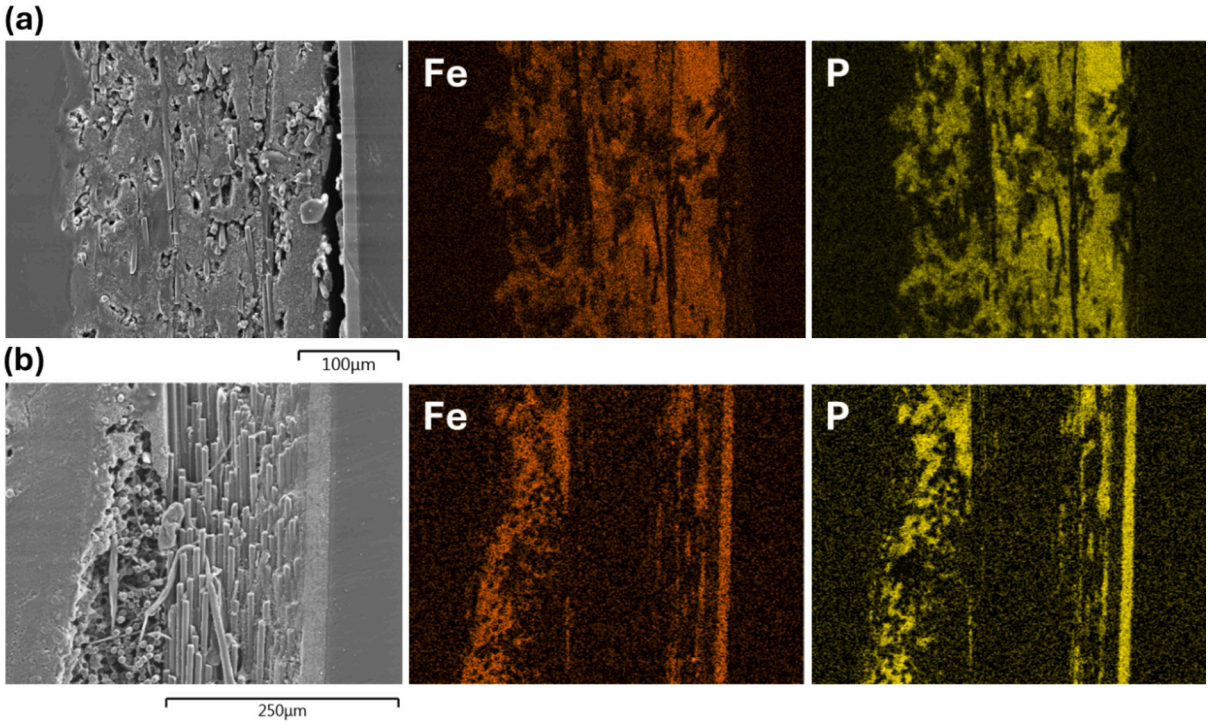

Fig. 7. (a) Cross-sectional SEM images of (a) reclaimed non-woven and (b) twill-weave composite cathodes and corresponding EDX elemental mapping images of Fe and P.

non-woven cathode exhibited a low **Rs** of 15.78 Ω, further evidence of superior dispersion of the conductive carbon black and a well-connected composite network. In contrast, the woven cathode showed a higher Rs of 28.29 Ω, consistent with lower percolation of the conductive network and a limited electronic pathway throughout the electrode.

$\mathbf{R_1}$ reflects the combined ionic and electronic resistance at the electrode-electrolyte interface and is influenced by the accessibility of the LFP and carbon continuity. Again, the non-woven reclaimed carbon fabric outperformed the woven fabric with $\mathbf{R_1}$ values of 62.67 Ω and 850.6 Ω, respectively. The charge-transfer resistance ($\mathbf{R_{ct}}$), the kinetic barrier for lithium-ion intercalation at the LFP surface, largely governed by accessibility and dispersion of the LFP particles and the electrolyte ionic conductivity was 40.25 Ω and 851.1 Ω, for the non-woven and woven electrodes, respectively. For context, in these systems reported previously, $\mathbf{R_{ct}}$ is typically ~200 Ω [46,47]. The greatly restricted Warburg parameter of the woven cathode of 86.57 Ω $s^{-1/2}$ vs the non-woven 6.573 Ω $s^{-1/2}$ suggests an order of magnitude greater lithium diffusion for the latter. This is consistent with the galvanostatic cycling data, justifying the observation whereby the non-woven electrode-maintained capacity even at 2C, while the woven cathode experienced too high interfacial resistances at rates as low as C/2.

Taken together, these results validate our initial hypothesis: the disordered architecture of the non-woven recycled carbon fibre enabled more effective infiltration of the LFP–SPE slurry during composite fabrication, facilitating better ionic access and utilization of the active material. This structural advantage not only enhances cathodic performance but also extends to the anode, where the increased surface area and resin distribution of the non-woven electrodes promoted superior rate capability performance and electrolyte wetting. In contrast, the tightly packed woven structure restricted resin penetration, limiting both ionic transport and electrochemically active surface area, as demonstrated by EIS and the rate capacity measurements. By integrating

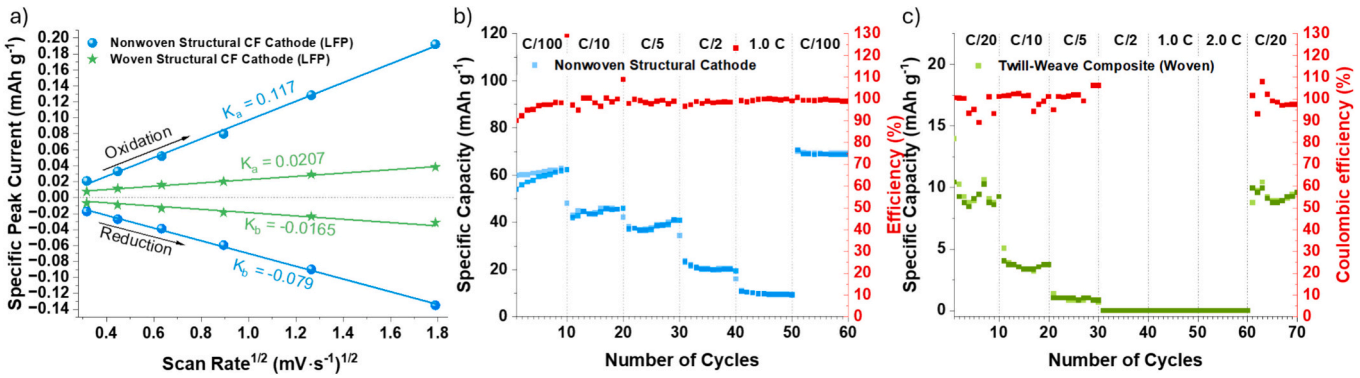

Fig. 8. (a) Randles–Ševčík plots of the non-woven and twill-weave carbon fibre composite cathodes. Galvanostatic cycling performance of the (b) non-woven and (c) twill-weave composites at various C-rates.

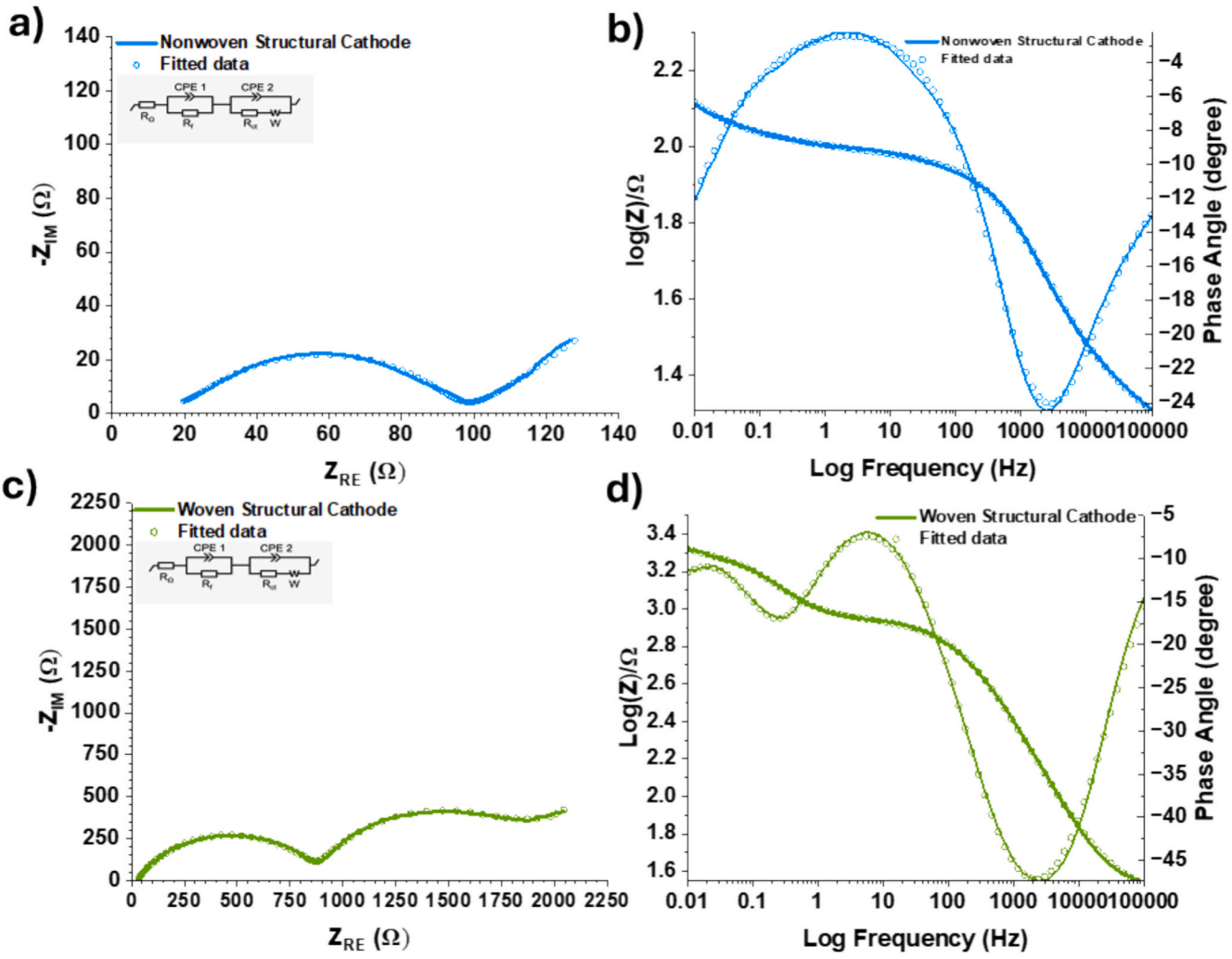

Fig. 9. Electrochemical impedance spectra of the non-woven cathode composite: (a) Nyquist and (b) Bode plots. Twill-weave cathode composite: (c) Nyquist and (d) Bode plots measured between 100 kHz to 10 mHz.

LFP directly into a percolated conductive network within the structural electrolyte, the recycled non-woven fabrics can serve as a scalable and high-performing electrode platform—offering a promising route toward multifunctional structural energy storage without compromising composite integrity or manufacturability.

3.4. All-fibre structural full cells using hybrid textile lamination

Building on the demonstrated electrochemical advantages of the recycled non-woven carbon fabric in both anode and cathode roles, we developed an all-fibre structural full cell by pairing a non-woven cathode with a twill-weave carbon fibre anode. This hybrid textile architecture allows a high active material loading with ionic accessibility

attributed to the non-woven composite cathode to be combined with the inherent alignment and mechanical reinforcement potential of the twill-weave composite anode. It is worth noting that our attempts to make a symmetrical full cell with non-woven materials often led to puncture of the separator, due to the entangled nature and high stiffness of the reclaimed material. This challenge will be addressed in future works.

Nevertheless, the resulting structural composite offers a promising path toward multifunctionality with integrated energy storage and strength. A key challenge facing structural batteries is the reliance on inert atmospheres or dry room conditions during fabrication, which poses a significant barrier to scalable implementation. To address this, we sought to evaluate the structural full cell fabrication process with conventional composite manufacturing workflows, including exposure to open-air environments between stages. Our targeted approach involves structural battery 'prepregs' that are partially cured—minimizing resin flow between layers while maintaining ionic transport pathways and limiting moisture uptake in the final vacuum cure. This would allow composite end users to enjoy the simplicity of industry suited thermoset laminate prepregs; simply cutting and moulding the material into the desired shape, facilitating scalable and practical implementation of a structural battery in real-world applications. Therefore, we developed structural full cells by first coating the anode and cathode resin onto carbon fibres and allowing to vacuum-cure for 4 h. This was then followed by full cell assembly with a battery grade cellulose separator in-between the partially cured electrodes. After curing for 48 h under vacuum, the final cell was sealed in an aluminium pouch. Of particular importance is the length of time for the partial cure and the choice of separator. This is because one of the most frequent challenges encountered was the shorting of the cell during the final full cell assembly step. This occurred due to the migration of carbon black from the top layer (LFP cathode) through the separator and toward the anode. A cure time of 4 h suppressed this effect in most cases. However, the presence of stray carbon fibres or fibre puncture through the separator also lead to cell shorting. The latter is a common problem encountered in structural composite fabrication, which can be overcome with a more streamlined and automated prepreg manufacturing process [39]. Polypropylene separators are durable and can readily mitigate fibre shorting, however bond poorly to the final cured SBE matrix. As such, a cellulose separator (29 um thickness, battery grade) was selected that offered good adhesion to the resin and sufficient shorting suppression. Another crucial factor to battery performance is the balancing of the active materials, typically with the anode being in slight excess (~5–10 %). Having too much anode material results in lithium depletion during SEI formation and can greatly affect SEI stability and resistance build-up. However, carbon fibre composites typically have densities between 200 and 800 g per square meter (GSM), meaning that the amount of active material can range from 20 to 80 mg cm^{-2} [48,49]. To match even the lowest GSM estimates in a structural battery, approximately 40 mg cm^2 of LFP particles are needed to balance the cell. We are far from achieving such active material loadings in commercial cells, though recent state-of-the-art high-loaded LFP cathodes have been demonstrated with loadings as high as 100–115 mg cm^{-2} [50,51]. Recent studies have also somewhat navigated this problem by spreading a unidirectional tow over a larger surface area (i.e. 6 k filaments spread over 1–3 cm) [39,52–54], however scale-up requires repeated handling and stacking of plys to achieve meaningful mechanical properties at scale (increasing the risk of shorting), alongside resin consolidation issues. As a consequence, obtaining a balanced structural full cell with high active material loading, fibre adhesion to the SBE and cathode particles, and fibre textile architecture (such as weave pattern and loading) are standing challenges that need to be overcome in order to realize the full potential of structural batteries [23].

Nevertheless, the composite full cell reported herein (Fig. 10a), assembled in air, utilized 325 GSM twill-weave carbon fibre as the anode over a surface area of 4 cm^2 (130 mg) and 18 mg of LFP active material, distributed throughout the structural cathode electrode. This resulting cell has a cathode to anode density ratio of 7:1. Despite this, the performance of these cells at C/20 show an initial capacity of 25 mAh g^{-1},

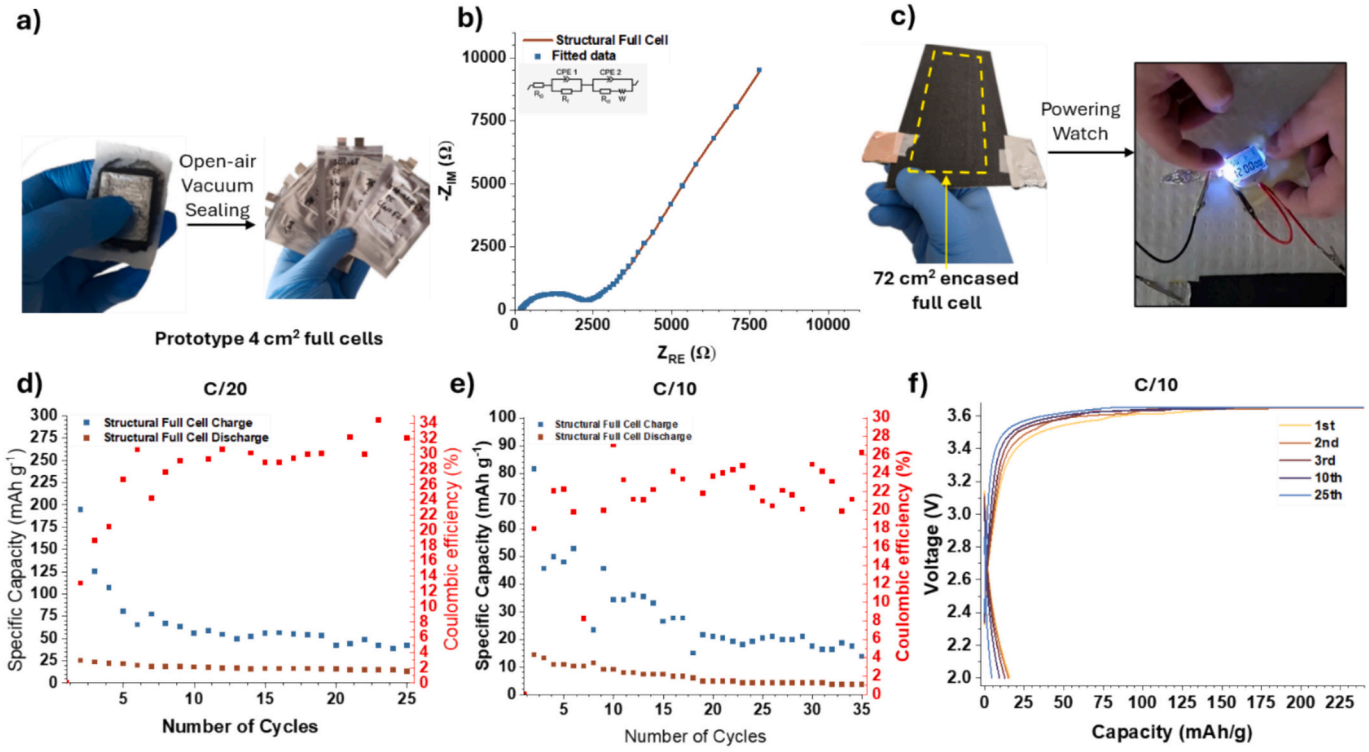

Fig. 10. (a) Structural full cells after vacuum bagging are further sealed in aluminium pouches to prevent moisture ingress into the composite. (b) Electrochemical Impedance Spectroscopy (EIS) of structural full cell after stabilization (c) Large-scale demonstration of a 72 cm^2 structural battery, see ESI for video. Cycling at various rates (d) C/20 and (e) C/10. Voltage capacity profile at C/10 (f).

which stabilized to 13 mAh g^{-1} after 25 cycles. Likewise at C/10 charging rate, an initial discharge capacity of 17 mAh g^{-1} was observed, reducing to 3.5 mAh g^{-1} after 35 cycles (Fig. 10e). The coulombic efficiency in these systems stabilizes at approximately 25 %, which suggests constant electrolyte breakdown and high resistances, and can be seen in the corresponding impedance data (Fig. 10b). Bulk resistance **Rs** was found to be around 183.8 Ω and charge transfer **Rct** approximately 2064 Ω, indicating sluggish interface kinetics. This was further evidenced by the high Warburg parameter; 1218 Ω $s^{-1/2}$, indicating very poor Li^+ diffusion. It is also likely that moisture ingress due to the open-air assembly had a negative role in cell performance, as this can lead to excessive electrolyte breakdown and unwanted side reactions. However, to do so whilst achieving comparable capacities over repeated cycles is a significant step forward.

While there remains room for improvement, particularly in terms of capacity and coulombic efficiency, the reported proof-of-concept open-air assembled composite structural battery successfully utilizes the entire carbon fibre network within the composite and demonstrates charge storage within an integrated solid-state electrolyte matrix. This approach is also scalable, with a 72 cm^2 laminate prepared and demonstrated powering a small device (Fig. 10b), offering great potential should the fabrication challenges be overcome.

3.5. Multifunctional performance

Evaluation of the resulting structural battery composites mechanical properties show the potential for multifunctionality, with the full-cell SBE exhibiting an energy of density of ~16.6 Wh/kg (Fig. 11a). The stiffer, though heavier full cell that was encased between CF laminates resulted in an energy density of ~6.5 Wh/kg. Further improvements in the energy density can be achieved by employing hot-pressing methods to extract more resin from the composite and through the development of thinner and more mechanically robust separators, which is an avenue for future work.

Mechanical evaluation of the structural full cell's reveals a tensile strength and Elastic Modulus of 33.1 ± 12.0 MPa and 859.3 ± 126.8 MPa respectively, whereas encasing within a carbon fibre epoxy laminate resulted in a 6-fold increase in tensile strength (201 ± 16.3 MPa) and 4-fold increase in Elastic Modulus (3.5 ± 0.29 GPa). Further increases in Elastic Modulus can readily be achieved by employing unidirectional (U·D) carbon fibres, owing to the superior stiffness and load-bearing properties (Fig. 11b). However, woven carbon fibres offer better conformability to complex geometries, superior isotropic in-plane strength and impact resistance. In targeted applications (such as automotive side panels or monocoques) both U·D and woven carbon fibre structural battery composites are required to achieve maximum performance. It is interesting to note that the flexural strength did not improve after encasing in the epoxy, this is because the encased cells experienced premature failure due to delamination of the internal cell during testing. As a result, flexural strength between the full cell and the encased cell was 39.66 ± 9.9 MPa and 41.4 ± 30.4 MPa, respectively. The flexural modulus between the full cell and the encased cell was 3.60 ± 1.0 GPa, whereas the encased flexural modulus dropped to 1.19 ± 0.33 GPa. Therefore, in our systems, reinforcing the cell by encasing between carbon fibre improved the tensile strength and Young's modulus and is a good path to improve stiffness, however, did not improve the flexural strength of flexural modulus due to premature delamination.

4. Conclusions

This work presents a novel, fully scalable, glovebox-free method for fabricating structural batteries using a prepreg-inspired approach. By leveraging an epoxy-IL electrolyte system and industry-standard composite layup techniques, we evaluate the electrochemical performance of the structural full cells, whilst also achieving large-scale laminate integration. While limitations in active material balancing currently constrain performance—manifesting as modest capacity and low coulombic efficiency—the approach leverages the full volume of the composite, avoids reliance on dry room conditions, and is inherently compatible with existing composite workflows. Electrochemical characterization confirms effective lithium transport and represents a significant step toward real-world implementation of structural batteries at scale, enabling lightweight, multifunctional energy storage solutions for aerospace, automotive, and beyond. Continued refinement of electrode balancing, separator integration, and electrolyte stability will be essential to advance these structural batteries toward commercial viability.

Supplementary data to this article can be found online at https://doi.org/10.1016/j.cej.2025.166504.

CRediT authorship contribution statement

James D. Randall: Writing – review & editing, Writing – original draft, Visualization, Methodology, Investigation, Formal analysis, Data curation. **Aqeel Muhammad:** Writing – original draft, Formal analysis, Data curation. **Emma G. Hogan:** Formal analysis, Data curation. **Timothy Harte:** Formal analysis, Data curation. **Žan Simon:** Writing – review & editing, Visualization, Formal analysis, Data curation. **Bhagya Dhamarsiri:** Writing – review & editing, Writing – original draft, Visualization, Supervision, Methodology. **Leif E. Asp:** Writing – review & editing, Funding acquisition. **Luke C. Henderson:** Writing – review &

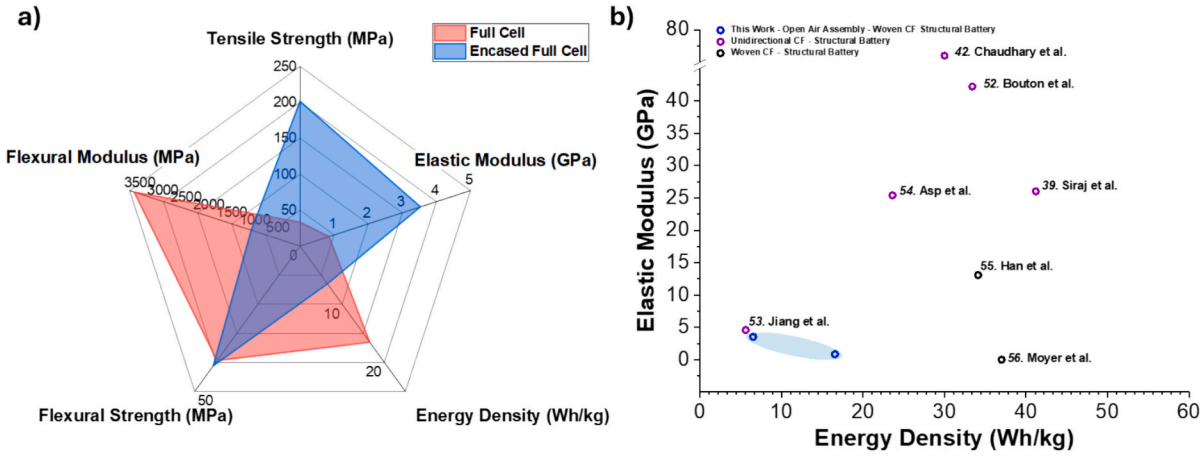

Fig. 11. (a) Radar Plot of mechanical data (tensile strength, elastic modulus, flexural strength, flexural modulus and energy density) of structural full cells, (b) Energy density and elastic modulus of reported structural batteries [39,52–56].

editing, Supervision, Project administration, Funding acquisition, Conceptualization.

Declaration of competing interest

The authors declare that they have no known competing financial interests or personal relationships that could have appeared to influence the work reported in this paper.

Acknowledgements

The authors gratefully acknowledge Deakin University, this research was conducted with support from the Australian Research Council Industry Transformation Research Hub (IH210100023), Discovery Projects (DP180100094, DP200100090, and DP230100587), and an IM Fellowship (IM230100048) for LH. This work was also partially supported by the Office of Naval Research (N62909-22-1-2052). The authors also acknowledge the facilities, and the scientific and technical assistance, of Microscopy Australia (formerly known as AMMRF) and the Australian National Fabrication Facility (ANFF). Gen2Carbon is thanked for providing reclaimed fiber fabrics.

The authors gratefully acknowledge the Deakin Electron Microscopy facility for support and assistance in this work. Leif Asp acknowledges funding from the Office of Naval Research, ONR, Contract No. N62909-22-1-2035.

Data availability

Data will be made available on request.

References

[1] D.V. Pelegov, J.-J. Chanaron, Electric car market analysis using open data: sales, volatility assessment, and forecasting, Sustainability 15 (1) (2023) 399.
[2] C.-W. Su, et al., Can new energy vehicles help to achieve carbon neutrality targets? J. Environ. Manag. 297 (2021) 113348.
[3] X. Yuan, X. Liu, J. Zuo, The development of new energy vehicles for a sustainable future: a review, Renew. Sust. Energ. Rev. 42 (2015) 298–305.
[4] S.T. Fuller, et al., Engineering electrodeposition for next-generation batteries, Electrochem. Soc. Interface 33 (2) (2024) 55.
[5] F.M.N.U. Khan, et al., Maximizing energy density of lithium-ion batteries for electric vehicles: a critical review, Energy Rep. 9 (2023) 11–21.
[6] M. Armand, et al., Lithium-ion batteries – current state of the art and anticipated developments, J. Power Sources 479 (2020) 228708.
[7] P.H. Camargos, et al., Perspectives on Li-ion battery categories for electric vehicle applications: a review of state of the art, Int. J. Energy Res. 46 (13) (2022) 19258–19268.
[8] Y. Wan, J. Takahashi, Development of carbon fiber-reinforced thermoplastics for mass-produced automotive applications in Japan, J. Compos. Sci. 5 (3) (2021) 86.
[9] D. Ozkan, M.S. Gok, A.C. Karaoglanli, Carbon Fiber Reinforced Polymer (CFRP) composite materials, their characteristic properties, industrial application areas and their machinability, in: A. Öchsner, H. Altenbach (Eds.), Engineering Design Applications III: Structures, Materials and Processes, Springer International Publishing, Cham, 2020, pp. 235–253.
[10] H. Ahmad, et al., A review of carbon fiber materials in automotive industry, IOP Conf. Ser. Mater. Sci. Eng. 971 (3) (2020) 032011.
[11] L.E. Asp, et al., Structural battery composites: a review, Funct. Compos. Struct. 1 (4) (2019) 042001.
[12] F. Danzi, et al., Structural batteries: a review, Molecules 26 (2021), https://doi.org/10.3390/molecules26082203.
[13] T. Jin, et al., Structural batteries: advances, challenges and perspectives, Mater. Today 62 (2023) 151–167.
[14] X. Chen, et al., Rigid structural battery: progress and outlook, J. Energy Storage 91 (2024) 112070.
[15] W. Johannisson, D. Zenkert, G. Lindbergh, Model of a structural battery and its potential for system level mass savings, Multifunct. Mater. 2 (3) (2019) 035002.
[16] S. Verma, B. Balasubramaniam, R.K. Gupta, Recycling, reclamation and re-manufacturing of carbon fibres, Curr. Opin. Green Sustain. Chem. 13 (2018) 86–90.
[17] S. Termine, et al., Investigation of carbon fibres reclamation by pyrolysis process for their reuse potential, Polymers 15 (2023), https://doi.org/10.3390/polym15030768.
[18] J.F. Snyder, E.L. Wong, C.W. Hubbard, Evaluation of commercially available carbon fibers, fabrics, and papers for potential use in multifunctional energy storage applications, J. Electrochem. Soc. 156 (3) (2009) A215.
[19] J. Hagberg, S. Leijonmarck, G. Lindbergh, High precision coulometry of commercial PAN-based carbon fibers as electrodes in structural batteries, J. Electrochem. Soc. 163 (8) (2016) A1790.
[20] T. Iijima, K. Suzuki, Y. Matsuda, Electrodic characteristics of various carbon materials for lithium rechargeable batteries, Synth. Met. 73 (1) (1995) 9–20.
[21] N. Zhang, et al., 4.6 V moisture-tolerant electrolytes for lithium-ion batteries, Adv. Mater. 36 (50) (2024) 2408039.
[22] M. Kosfeld, B. Westphal, A. Kwade, Moisture behavior of lithium-ion battery components along the production process, J. Energy Storage 57 (2023) 106174.
[23] N.A.A. Sutrisnoh, et al., Structural cathodes: navigating the challenges in fabrication and multifunctional performance analysis, Compos. Sci. Technol. 242 (2023) 110147.
[24] J. Ye, et al., Carbon fiber reinforced structural battery composites: progress and challenges toward industrial application, Compos. Part B Eng. 277 (2024) 111411.
[25] P. Liu, E. Sherman, A. Jacobsen, Design and fabrication of multifunctional structural batteries, J. Power Sources 189 (1) (2009) 646–650.
[26] R. Chaudhary, et al., High-energy cathode in carbon fibre structural battery, Compos. B: Eng. (2025) 112629.
[27] N.A.A. Sutrisnoh, et al., From properties to performance: understanding the multifunctional performance of carbon fiber cathodes for structural batteries, Compos. A: Appl. Sci. Manuf. 190 (2025) 108696.
[28] A. Balducci, Ionic liquids in lithium-ion batteries, in: B. Kirchner, E. Perlt (Eds.), Ionic Liquids II, Springer International Publishing, Cham, 2018, pp. 1–27.
[29] H. Niu, et al., Recent advances in application of ionic liquids in electrolyte of lithium ion batteries, J. Energy Storage 40 (2021) 102659.
[30] T. Harte, et al., Closing the loop: recyclable solvate ionic liquids in solid polymer electrolytes for circular economy, ACS Sustain. Chem. Eng. 12 (43) (2024) 16114–16125.
[31] T. Harte, et al., Bicontinuous solid polymer electrolytes using Li+ enriched ionic liquids, J. Mol. Liq. 402 (2024) 124689.
[32] Ž. Simon, et al., From stress to charge: investigating the piezoelectric response of solvate ionic liquid in structural energy storage composites, Mater. Horiz. 11 (18) (2024) 4321–4328.
[33] X. Xiang, K. Zhang, J. Chen, Recent advances and prospects of cathode materials for sodium-ion batteries, Adv. Mater. 27 (36) (2015) 5343–5364.
[34] D. Alvira, D. Antorán, J.J. Manyà, Assembly and electrochemical testing of renewable carbon-based anodes in SIBs: a practical guide, J. Energy Chem. 75 (2022) 457–477.
[35] Q. Zhuang, et al., Studies of the first lithiation of graphite materials by electrochemical impedance spectroscopy, Chin. Sci. Bull. 51 (9) (2006) 1055–1059.
[36] X. Zhao, et al., Influence of electrolytic cell system on graphite electrode interface properties, J. Phys. Conf. Ser. 2468 (1) (2023) 012106.
[37] S. Pei, et al., Evolutionary mechanism and frequency response of graphite electrode at extreme temperatures, Nano Res. 17 (8) (2024) 7283–7289.
[38] J. Xu, et al., A multicell structural battery composite laminate, EcoMat 4 (3) (2022) e12180.
[39] M.S. Siraj, et al., Advancing structural battery composites: robust manufacturing for enhanced and consistent multifunctional performance, Adv. Energy Sustain. Res. 4 (11) (2023) 2300109.
[40] S. Termine, et al., Investigation of carbon fibres reclamation by pyrolysis process for their reuse potential, Polymers 15 (3) (2023) 768.
[41] J. Hagberg, et al., Lithium iron phosphate coated carbon fiber electrodes for structural lithium ion batteries, Compos. Sci. Technol. 162 (2018) 235–243.
[42] R. Chaudhary, et al., Unveiling the multifunctional carbon fiber structural battery, Adv. Mater. 36 (48) (2024) 2409725.
[43] J. Szecsödy, Electrochemical characterisation of LiFePO4-coated carbon fibres: a comparative electrochemical analysis of three coating methods, in: TRITA-CBH-GRU, 2023.
[44] G. Guzmán, et al., Improved performance of LiFePO4 cathode for Li-ion batteries through percolation studies, Electrochim. Acta 247 (2017) 451–459.
[45] K. Yuelin, et al., Efficient separation and selective Li recycling of spent LiFePO4 cathode, Energy Mater. 3 (6) (2023) 300053.
[46] J. Choi, et al., Advancing structural batteries: cost-efficient high-performance carbon fiber-coated LiFePO4 cathodes, RSC Adv. 13 (44) (2023) 30633–30642.
[47] R. Chaudhary, et al., Structural positive electrodes engineered for multifunctionality, Adv. Sci. 11 (33) (2024) 2404012.
[48] M. Andreozzi, et al., Effect of fabric areal weight on the mechanical properties of composite laminates in carbon-fiber-reinforced polymers, J. Compos. Sci. 7 (9) (2023) 351.
[49] C. Tosto, et al., Comparison of carbon-reinforced composites manufactured by vacuum assisted resin infusion with traditional and fully recyclable epoxy resins, Polym. Compos. 45 (17) (2024) 15649–15663.
[50] C. de la Torre-Gamarra, et al., High mass loading additive-free LiFePO4 cathodes with 500 μm thickness for high areal capacity Li-ion batteries, J. Power Sources 458 (2020) 228033.
[51] X. Zhang, et al., Ultrahigh-mass-loading flexible LiFePO4 cathode with the drop-shaped low-tortuosity architecture for high-performance flexible lithium-ion batteries, J. Colloid Interface Sci. 690 (2025) 137320.
[52] K. Bouton, et al., A structural battery with carbon fibre electrodes balancing multifunctional performance, Compos. Sci. Technol. 256 (2024) 110728.
[53] Q. Jiang, et al., Structural composite batteries made from carbon fibre reinforced electrodes / polymer gel electrolyte prepregs, Compos. Sci. Technol. 244 (2023) 110312.

[54] L.E. Asp, et al., A structural battery and its multifunctional performance, Adv. Energy Sustain. Res. 2 (3) (2021) 2000093.
[55] Z. Han, et al., Manufacturing carbon fabric composite structural batteries using spray with high-pressure and high-temperature and vacuum-bag assisted infusion techniques, Compos. Sci. Technol. 245 (2024) 110321.
[56] K. Moyer, et al., Carbon fiber reinforced structural lithium-ion battery composite: multifunctional power integration for CubeSats, Energy Storage Mater. 24 (2020) 676–681.